Encapsulation of two-dimensional materials inside carbon nanotubes: towards an enhanced synthesis of single-layered metal halides

Stefania Sandoval,[1] Elzbieta Pach,[2] Belén Ballesteros*[2] and Gerard Tobias*[1]

[1] Institut de Ciència de Materials de Barcelona (ICMAB-CSIC), Campus de la UAB, 08193 Bellaterra, Barcelona, Spain.

[2] Catalan Institute of Nanoscience and Nanotechnology (ICN2), CSIC and The Barcelona Institute of Science and Technology, Campus UAB, Bellaterra, 08193 Barcelona, Spain

*Corresponding author. E-mail: gerard.tobias@icmab.es (Gerard Tobias); belen.ballesteros@icn2.cat (Belén Ballesteros).

Abstract

The unique properties of two-dimensional (2D) nanomaterials make them highly attractive for a wide range of applications. As a consequence, several top-down and bottom up approaches are being explored to isolate or synthesize single-layers of 2D materials in a reliable manner. Here we report on the synthesis of individual layers of several 2D van der Waals solids, namely CeI_3, $CeCl_3$, $TbCl_3$ and ZnI_2 by template-assisted growth using carbon nanotubes as directing agents, thus proving the versatility of this approach. Once confined, the metal halides can adopt different structures including single-layered metal halide nanotubes, which formation is greatly enhanced by increasing the temperature of synthesis. This opens up a new strategy for the isolation of individual layers of a wide variety of metal halides, a family of 2D materials that has been barely explored.

1. Introduction

The formation of low dimensional systems is a powerful tool for tuning the physical properties of materials. As a consequence, a wide variety of approaches have been explored to synthesize and control their size, morphology and crystal structure. Template-directed synthesis represents a convenient and versatile route for the growth of low dimensional systems and both organic and inorganic-based materials are being employed as templates. In this sense, carbon nanotubes (CNTs) are an attractive host since they can have a variety of diameters and lengths and their inner hollow cavity can be filled with a large variety of compounds.[1-6] Among them, metal halides have received widespread attention since the resulting hybrids are of interest for instance for biomedical imaging [7-9], even allowing mapping of cellular organelles.[10] In general, confinement of materials within the walls of CNTs results in the formation of molecular entities, nanoclusters or nanowires. For the vast majority of applications removal of the carbon template is not desired since the resulting hybrid typically presents a high stability. Furthermore, the presence of CNTs might create synergistic effects with the filling material resulting in unique properties and superior performance.[11] Actually, the application of filled CNTs expands from molecular magnets[12] to biomedicine[13] going through sensors[14]. More recently, the possibility of isolating individual layers of two-dimensional (2D) materials inside CNTs has attracted a great deal of attention. Nanoribbons of graphene[15] and metal dichalcogenides (MoS_2, WS_2)[16] have been synthesized within the cavities of single- and double-walled CNTs, whereas single-layered PbI_2 nanotubes have been grown using multi-walled CNTs as templates.[17] A recent theoretical study by Zhou et al. reveals that these heterostructures, consisting of single-layers of PbI_2 and a carbon layer can substantially enhance the visible light response, suggesting potential applications in novel 2D optoelectronics and

3

photovoltaics.[18] Despite their interest, the number of reports on single-walled inorganic nanotubes is limited because the formation of their multi-walled counterparts is favored during the synthesis.[19] Therefore, the possibility of growing single-layered nanotubes using CNTs as directing agents opens up a new synthetic strategy for the development of advanced nanomaterials that combine the characteristics of both 1D and 2D systems.[20] Here we show that the templating strategy is versatile by reporting on the synthesis of single-layered nanotubes of $TbCl_3$, CeI_3, $CeCl_3$ and ZnI_2. Furthermore, by controlling conditions of the synthesis it is possible to enhance the formation of these single layered structures. The present approach expands the strategies available for the isolation and growth of individual layers of 2D van der Waals solids, which can go via bottom-up (e.g. chemical vapor deposition) and top down (e.g. liquid phase exfoliation) approaches.[21, 22] Among the different morphologies that 2D materials can adopt, the formation of nanoscrolls,[23] concentrically rolled-up 2D layers, is getting an increased attention. For instance, highly thermal-stable paramagnetism has been recently reported by rolling up MoS_2 nanosheets,[24] and an enhanced photon absorption has been observed in spiral nanostructured solar cells. [25] The formation of nanoscrolls also opens up new opportunities in composite materials.[26] When both longitudinal edges of an individual 2D nanoscroll are seamlessly joined, a single-layered nanotube is formed, typically referred to as single-walled nanotube. The concept of using edgeless 2D rolled-up sheets is for instance being investigated for the development of ultracompact plasmon circuitry at the nanoscale because plasmons along 2D ribbons suffer from scattering at edges.[27]

Noteworthy, within the several families of van der Waals solids, metal halides have received little attention when it comes to the individualization of their constituent layers and will be the focus of the present study.

2. Experimental

2.1 Filling of MWCNTs with $TbCl_3$, $CeCl_3$, CeI_3 and ZnI_2

Multiwalled carbon nanotubes (CVD, Thomas Swan Co.Ltd.) were steam treated in order to remove amorphous carbon and graphitic nanoparticles and to open their ends.[28] Additionally, the sample was treated with a 6 M HCl solution to remove the catalytic metal nanoparticles,[29] filtered and dried overnight at 60 ºC. In an argon-filled glove box, purified CNTs and the corresponding salt ($TbCl_3$, CeI_3, $CeCl_3$ or ZnI_2) were ground with an agate mortar and pestle until the mixture presented a uniform color. The mixture was then transferred into a silica ampoule, evacuated and sealed under vacuum. The ampoule was placed into a furnace where it dwelled at temperatures above the melting point of the salt, during 12 hours. The respective temperature was obtained after a controlled heating rate (5 ºC.min^{-1}). Finally, the samples were cooled at 0.42 ºC.min^{-1} until temperatures under the melting point and subsequently at 5 ºC.min^{-1} until room temperature. In order to tailor the nature of the inner structure obtained inside the template, ZnI_2 was treated at temperatures ranged between 475 ºC and 1000 ºC. Time of treatment and heating ramp were kept constant (12 h and 5 ºC.min^{-1}, respectively).

2.2 Characterization

The morphology and the distribution of the inorganic structures grown within the MWCNTs was studied recording TEM, HRTEM images and high-angle annular dark field (HAADF) images in scanning transmission electron microscopy (STEM) mode. TEM images were obtained using a JEOL 1210 microscope, operating at 120 kV. HRTEM was carried out in a FEI Tecnai F20 microscope operating at 200 kV. Samples were prepared by sonicating and dispersing in hexane. Afterwards, they were placed

5

dropwise onto a lacey carbon coated Cu support grid. EDX analysis was performed on a FEI Quanta SEM by placing the Cu grid on top of an aluminium support.

3. Results and Discussion

Single-layered nanotubes of several 2D van der Waals solids, namely $TbCl_3$, CeI_3, $CeCl_3$ and ZnI_2, were prepared by molten phase capillary wetting,[30] using steam purified and open-ended multiwalled CNTs (MWCNTs) as templates (see experimental details). A mixture of MWCNTs and the metal halide was annealed under vacuum at temperatures above the melting points of the selected materials (475 °C-1000 °C).[31] The successful formation of single-layered inorganic nanotubes was confirmed by analysis of the resulting sample by high-resolution transmission electron microscopy (HRTEM) and scanning transmission electron microscopy (STEM). Figure 1 shows a HRTEM image of a single-layered $TbCl_3$ nanotube synthesized within the cavity of a MWCNT at 650 °C. The metal halide layer is easily differentiated from the walls of the carbon nanotube due to the difference of contrast.
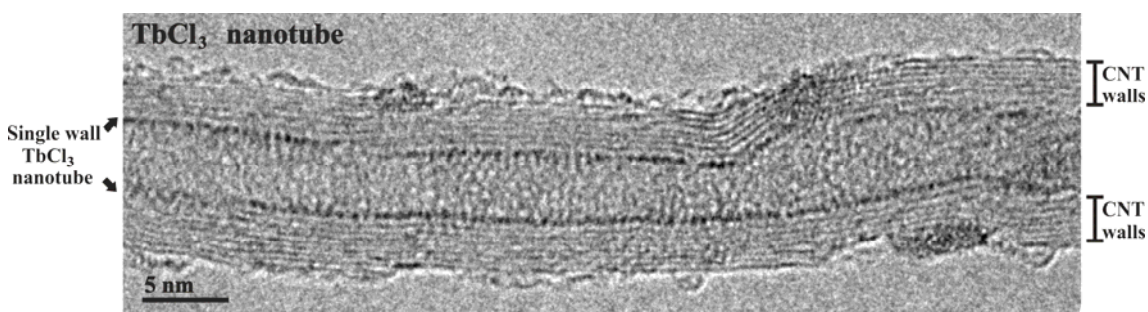

Figure 1. HRTEM image of $TbCl_3$ single-layered nanotube confined within a MWCNT.

Next, to provide evidence of the versatility of this approach, the growth of individual layers of cerium based 2D systems was attempted. CeI_3 and $CeCl_3$ were the materials of choice being filled at 900 °C and 850 °C respectively. Since the constituent elements of the employed salts are heavier than carbon (from CNTs) it is possible to easily discern the filling material by means of high-angle annular dark field (HAADF) STEM

imaging. The intensity of HAADF-STEM images (also called Z-contrast imaging) scales approximately with the square of the atomic number. Thus heavy elements, metal halides in our case, will appear brighter than light elements, such as carbon from the CNTs. Therefore, the bright lines observed in Figure 2 (a) and Figure S1 (a) along the inner walls of the CNTs can be attributed to the metal halides. The diameter of the inorganic nanotubes displayed in the HAADF-STEM images is in the range of 3.5-6.9 nm. The thermal annealing of metal halides in the presence of CNTs also results in the formation of other nanostructures inside the CNTs (Figure S2), which mainly take the form of nanorods but nanoparticles have also been observed inside few CNTs. When nanorods are present, these can either completely (Fig. S2 (a)) or partially (Fig. S2 (b)) fill the hollow cavity of the CNTs, the latter adopting a polycrystalline snake-type morphology. To discern between both types of structures we will refer to the former as nanorods and to the latter as "nanosnakes". In most cases crystalline structures are observed for the confined metal halides. The spacing of the lattice fringes in the HRTEM image of the CeI_3 nanorod in Figure S2 (a) is in good agreement with the (130) plane of bulk CeI_3 presenting an orthorhombic structure, thus confirming the successful encapsulation of this material.[32]
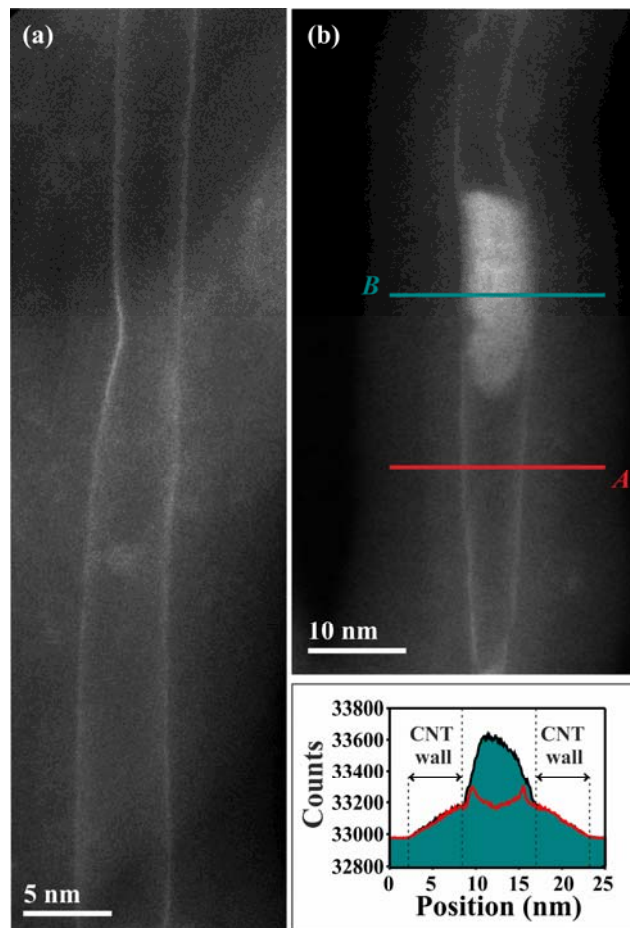
Figure 2. HAADF STEM images of (a) a CeI_3 inorganic single-layered nanotube confined within a MWCNT and (b) intensity profiles of two segments of a MWCNT containing a nanotube (*A*, red line) and a nanorod (*B*, green line) of CeI_3.

The coexistence of different types of inorganic nanostructures inside an individual CNT has also been observed. For instance, in Figure 2(b) a fragment of an inorganic nanorod of CeI_3 has grown within the walls of a single-layer nanotube of the same material. Both types of structures can be easily discerned by visual inspection of the Z-contrast STEM image (Figure 2 (b)), but further evidence can be provided by intensity profiles across an area presenting a single-layered inorganic nanotube (red line, *A*) and an area containing a nanorod fragment (green line, *B*). Marked differences between the intensity profiles become evident. When the inner nanorod is present, the highest intensity is detected in the central space of the analyzed area, confirming the complete filling of the

8

host. In contrast, the intensity profile of the tubular fraction shows the highest intensity at the edges, with a diameter and shape determined by the inner cavity of the carbon nanotube. A much weaker intensity is registered in the intensity profile of an empty area where only carbon, from the CNT walls, is present (blue line, *B*; Figure S3). Although most of the CNTs have opened ends, the presence of some closed tips has allowed the formation of CeI_3 caps which are visible in the Z-contrast STEM image in Figure S3. A clear differentiation between the inorganic nanotubes and nanorods is also visible by TEM analysis (Figure S4).

Temperature being a key factor in the molten filling process,[33] we decided to investigate the role of this parameter towards the formation of nanotubes and other types of nanostructures. Therefore we analyzed the encapsulation of CeI_3 at 800 °C and 900 °C. Interestingly, a remarkable increase in the amount of single-layered nanotubes is observed upon increasing the temperature of the synthesis (from 7.4 % at 800°C to 21.5% at 900 °C). To have statistically significant data, analysis of over 200 individual filled CNT was performed on each of the samples (Table 1); empty CNTs were not considered in this analysis. Figure S5 presents a detailed analysis of the different types of inner structures grown within the CNTs with respect to the temperature of the treatment (see Table S1 for numerical data). The sample of $CeCl_3$ is also included for comparison. In all the prepared samples inorganic nanotubes can be present as "short" (bubble like nanostructures <35 nm in length, Figure S6) or "long" nanotubes (length > 35 nm, Figure S1(a-c)), which are differentiated in the present analysis. In most cases short nanotubes were grown as at least three consecutive close ended hollow structures. For both materials, CeI_3 and $CeCl_3$, the presence of long nanotubes was clearly higher than short ones in all the prepared samples.

Table 1. Formation of inorganic nanotubes (in % frequency) versus other nanostructures in samples of CeI_3 filled MWCNTs (CeI_3@MWCNT) at two different temperatures.

Sample	Nanotubes (%)	Other nanostructures (%)
CeI_3@MWCNT, 800 ºC	7.4	92.6
CeI_3@MWCNT, 900 ºC	21.5	78.5

Taking into account that marked differences were observed by a mere increase in the temperature of synthesis, and in order to better understand the role of temperature on the formation of the different types of inorganic nanostructures, we next filled ZnI_2 into steam treated CNTs. Cerium halides have significantly high melting points, which limit the range of temperature at which these materials can be encapsulated. ZnI_2 was selected among the employed halides since it is also a layered van der Waals solid, it has the lowest melting point (446 °C) of all the materials investigated in this study, and a low surface tension of the melt.[34] The latter is a key parameter since liquids with low surface tensions will most readily wet the CNTs.[35] Moreover, the presence of the strongly scattering halogen (I, $Z= 53$) allows an easy differentiation of the grown structures by Z-contrast microscopy.[36, 37] Following the same protocol used for the Ce and Tb halides, a mixture of CNTs and ZnI_2 was annealed under vacuum at about 30 °C above the melting point of ZnI_2 (475 °C). The resulting sample was analyzed by HRTEM and STEM which allowed us to confirm the successful growth of single-layered ZnI_2 nanotubes confined inside the CNTs. Figure 3 (a) shows a representative STEM image of a ZnI_2@CNT. The intensity profile is in good agreement with the presence of a single-layered nanotube since a sharp and high intensity profile is observed following the inner walls of the CNT. In this case, the diameter of the ZnI_2

nanotubes is 5.6 nm. A schematic representation of a single-layered nanotube having the same diameter than the one observed in the experimental image is included in Figure 3 (b). EDX analysis confirms the presence of the constituent elements, Zn and I (Figure 3 (c)).
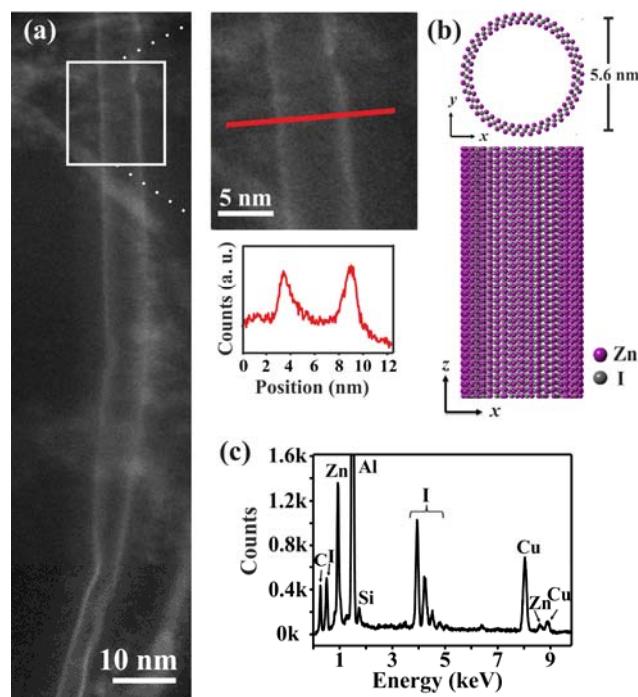

Figure 3. (a) HAADF STEM image of ZnI_2@MWCNTs with the respective intensity profile along the red line. (b) Schematic representation of a single-layered ZnI_2 nanotube with the diameter observed in the experimental image, projected along the main axis and cross section. (c) EDX analysis confirming the presence of both Zn and I in the sample along with C (from the CNTs); Al and Cu signal arise from the support employed for the analysis, whereas the Si peak could arise from the contact of the sample with the silica ampoule employed for the synthesis.

Actually the intensity profile across the main tube axis can also be employed to determine the thickness of the inner coating. HRTEM images of several encapsulated metal halides, namely ZnI_2, CeI_3 and TbI_3 are presented in Figure 4 along with the bulk structural model of the employed layered materials. The wall thickness determined by

11

means of intensity profiles is marked with white arrows in the HRTEM images. For ease of comparison, the unit cell is indicated with a black continuous line on the structural model, also including two of the lattice constants. The thickness of each constituent layer can be easily determined by dividing the value of the cell parameter perpendicular to the layers by the number of layers that it contains. In the case of ZnI_2 it is straight forward since in the represented CdI_2-type structure there is only one layer per unit cell.[38] Therefore, the thickness of each layer of ZnI_2 equals to that of the unit cell 0.654 nm,[39] which also accounts for the van der Waals spacing between layers. Both CeI_3 and $TbCl_3$ can crystallize with an orthorhombic $PuBr_3$-type structure with two layers per unit cell.[38] Thus, in this case the thickness of an individual layer would be 0.70 nm (14.00 Å / 2) for CeI_3[32] and 0.589 nm (11.774 Å / 2) for $TbCl_3$.[40] It is worth noting that regardless of the encapsulated material, the measured wall thickness in the HRTEM images, namely 0.45 nm (ZnI_2), 0.53 nm (CeI_3) and 0.40 nm ($TbCl_3$) are in good agreement with those of an individual layer of metal halide, 0.654 nm, 0.70 nm, 0.589 nm. As expected, in all cases the thickness determined by the intensity profile is slightly smaller than the one derived from the crystallographic data of bulk crystals since as mentioned, the latter also takes into account the van der Waals distance between subsequent layers. Also with the measured thicknesses we can clearly discard the presence of two or more layers of metal halides coating the inner cavities of the MWCNTs. From over 600 inorganic metal halide nanotubes observed in the present study (Table S1) only in one case we could detect the presence of an inorganic nanotube bearing more than one layer; a triple-walled nanotube of ZnI_2 (Figure S7). As it can be seen in the image the presence of a triple-walled nanotube can be easily discerned from the single-walled inorganic nanotubes analyzed so far. Actually both HRTEM and HAADF STEM have been previously used to assess the number of constituent layers of metal halides nanotubes. For instance, whereas PbI_2 has been reported to form single-

12

layered nanotubes inside the cavities of carbon nanotubes,[17] multi-walled PbI$_2$ nanotubes are formed when using WS$_2$ nanotubes as templates.[41]
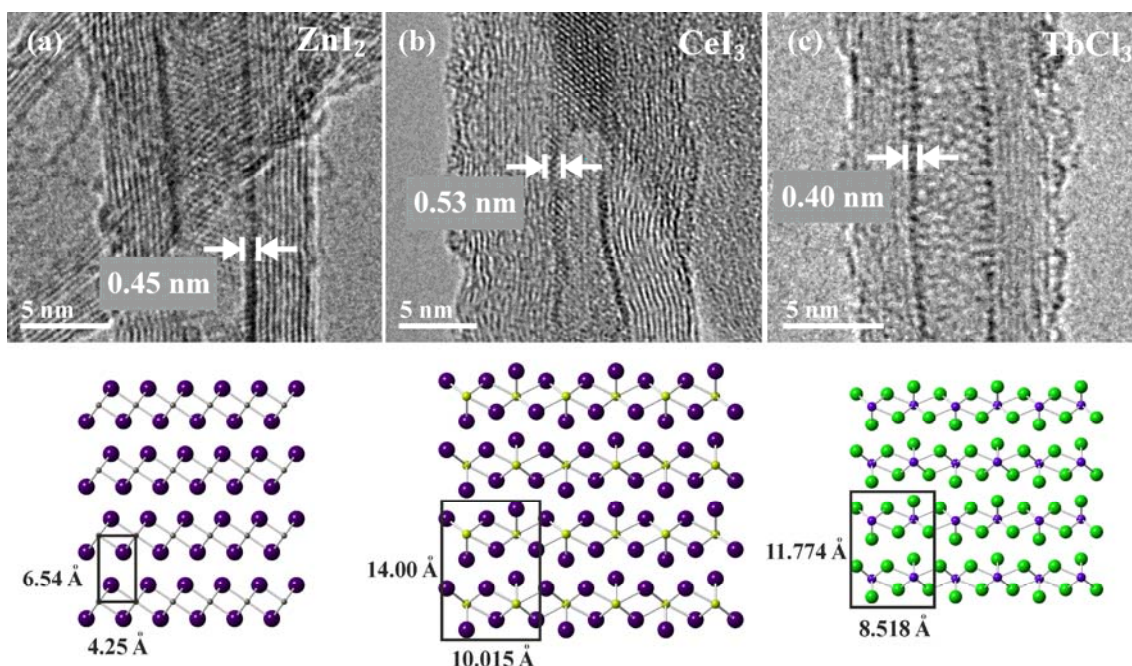

Figure 4. Top panel: HRTEM images of (a) ZnI$_2$@MWCNTs, (b) CeI$_3$@MWCNT and (c) TbCl$_3$@MWCNTs. Arrows point out the wall thickness of the encapsulated metal halides as determined by intensity profiles. Bottom panel: projection of the structural models of bulk (a) ZnI$_2$ (b) CeI$_3$ and (c) TbCl$_3$. Large spheres correspond to the halides (I or Cl) and small spheres to the metals (Zn, Ce, or Tb). The unit cell is indicated with a black continuous line on the structural model, also including two of the lattice constants.

To complete the study, and in order to further investigate the role of temperature on the formation of metal halide nanostructures, additional samples were prepared by annealing a mixture of ZnI$_2$ and CNTs at 575 ˚C, 700 ˚C and 1000 ˚C. The structure of the encapsulated compounds was determined on more than 190 filled nanotubes for each of the prepared samples (Table S1). As it can be seen in Table 2, an overwhelming increase on the amount of inorganic nanotubes is observed when increasing the

temperature of the synthesis, from 21.4 % (at 475 ˚C) up to 64.9 % (at 1000 ˚C). This corresponds to a threefold enhancement of the formation of single-layered nanotubes. Obviously, the continuous increase in the amount of ZnI_2 nanotubes upon increasing the temperature of synthesis results in a proportional decrease in the amount of other nanostructures present inside CNTs (Figure 5 (a)). This is in good agreement with the trend observed for CeI_3 nanotubes.

Table 2. Effect of the temperature of the synthesis towards the formation of ZnI_2 nanotubes or other nanostructures inside MWCNTs.

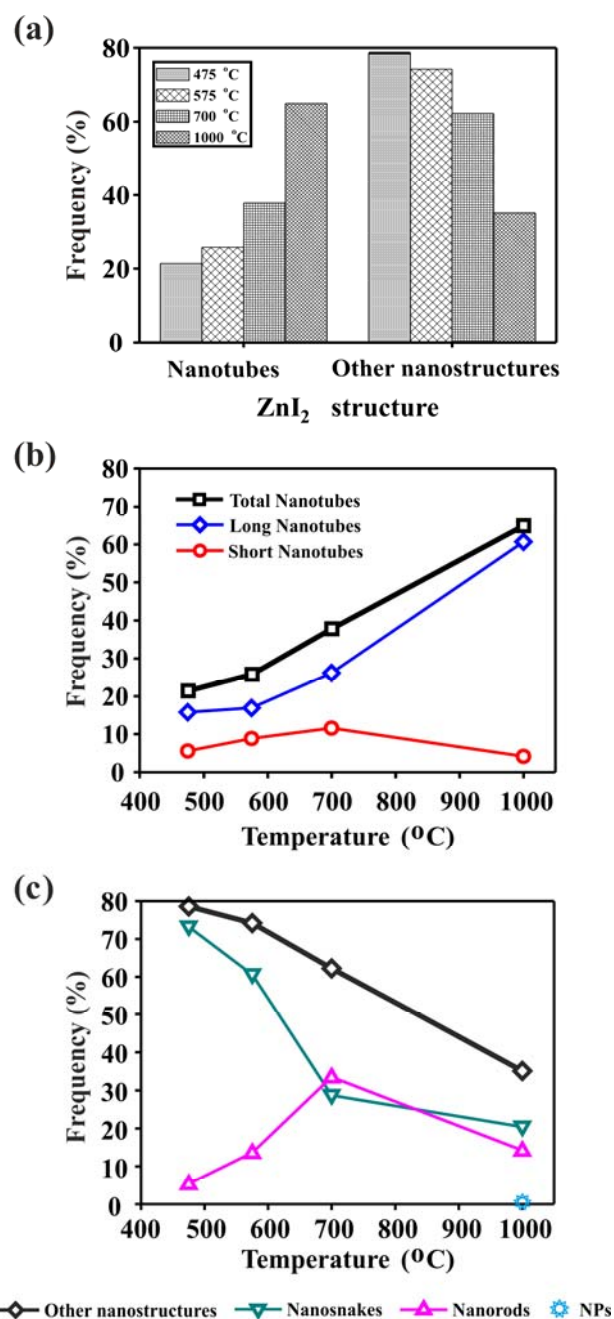| Temperature of filling	ZnI_2 inorganic nanotubes (%)	Other inorganic nanostructures (%)
475 ˚C	21.4	78.6
575 ˚C	25.8	74.2
700 ˚C	37.8	62.2
1000 ˚C	64.9	35.1

Fig. 5. (a) Bar diagram showing the distribution (frequency, %) of ZnI_2 nanotubes *versus* other structures grown inside MWCNTs (for numerical data see Table S1). (b) Detailed analysis on the effect of temperature towards the formation of ZnI_2 nanotubes, differentiating between long and short ones. (c) Role of temperature in the formation of other ZnI_2 nanostructures, different from inorganic nanotubes, namely nanorods, "nanosnakes" and nanoparticles (NPs).

If we now focus on the formation of inorganic nanotubes (Fig. 5 b)), again both long and short structures were also observed, with similar characteristics to the CeI_3 and $CeCl_3$ samples (Figures S1). Again the amount of long nanotubes was always higher than the amount of short nanotubes for a given sample. Interestingly, a different trend is observed for the formation of short and long inorganic nanotubes upon increasing the temperature of the synthesis. In the case of long nanotubes, an increase in temperature produced a significant and continuous increase in the frequency of long inorganic ZnI_2 nanotubes (from 15.8 % at 475 ˚C to 60.7 % at 1000 ˚C). In contrast, in the case of short nanotubes, although at lower temperatures there is also an increase towards the formation of this type of structures, an inflection point is clearly visible at 700 ˚C and the lowest amount of short nanotubes is recorded at 1000 ˚C (4.2 %). This implies that at 1000 ˚C not only the formation of inorganic nanotubes is favored over other nanostructures but also the ZnI_2 nanotubes obtained at this temperature will be longer than 35 nm (long nanotubes).

Apart from single-layered inorganic nanotubes, other nanostructures were also observed within the CNT cavities, mainly nanorods and "nanosnakes" (Fig 5(c), Figure S8). ZnI_2 inorganic nanoparticles were not observed in most of the samples, except for the sample treated at 1000 ˚C, where only a 0.5 % was detected (Table S1). As expected, and in agreement with the general trend observed for the other nanostructures in Figure 5 (a), the amount of "nanosnakes" decreases with increasing temperature of the treatment. Interestingly, again an inflection point is observed at 700 ˚C for the ZnI_2 nanorods which follows a similar trend than that found with short nanotubes, with a maximum at 700 ˚C (33.5 %) and registering an abrupt decrease for the sample treated at 1000 ˚C down to 14.2 %. The changes observed at 700 ˚C clearly deserve special attention. The fact that the filling process is taking place above the boiling point of ZnI_2 (625 ˚C)[31] might account for this, but further investigations are needed.

4. Conclusions

To conclude, individual layers of different 2D van der Waals solids, namely CeI_3, $CeCl_3$, $TbCl_3$ and ZnI_2 have been isolated and grown in the form of single-layered inorganic nanotubes inside MWCNTs. The formation of inorganic nanotubes of several metal halides containing different anions and cations provides direct evidence of the versatility that the inner cavities of the CNTs offer for the isolation of individual layers of 2D materials. The influence of the temperature of the treatment on the resulting nanostructure has been explored in detail. The higher the temperature of the synthesis the higher the amount of single-layered metal halide nanotubes formed inside the hosting template. The versatility of the presented approach further expands the synthetic approaches for the isolation and growth of individual layers of 2D materials.

References

[1]Monteiro AO, Costa PMFJ, Cachim PB, Holec D. Buckling of ZnS-filled single-walled carbon nanotubes – The influence of aspect ratio. Carbon 2014;79:529-37.
[2]Nie C, Galibert A-M, Soula B, Flahaut E, Sloan J, Monthioux M. A new insight on the mechanisms of filling closed carbon nanotubes with molten metal iodides. Carbon 2016;110:48-50.
[3]Torres-Dias AC, Cambré S, Wenseleers W, Machon D, San-Miguel A. Chirality-dependent mechanical response of empty and water-filled single-wall carbon nanotubes at high pressure. Carbon 2015;95:442-51.

[4]Monthioux M, Flahaut E, Cleuziou J-P. Hybrid carbon nanotubes: Strategy, progress, and perspectives. Journal of Materials Research 2006;21:2774-93.

[5]Cambré S, Campo J, Beirnaert C, Verlackt C, Cool P, Wenseleers W. Asymmetric dyes align inside carbon nanotubes to yield a large nonlinear optical response. Nat Nano 2015;10:248-52.

[6]Shao L, Tobias G, Huh Y, Green MLH. Reversible filling of single walled carbon nanotubes opened by alkali hydroxides. Carbon 2006;44:2855-8.

[7]Ma Q, Jebb M, Tweedle MF, Wilson LJ. The gadonanotubes: structural origin of their high-performance MRI contrast agent behavior. Journal of Materials Chemistry B 2013;1:5791-7.

[8]Rivera EJ, Tran LA, Hernandez-Rivera M, Yoon D, Mikos AG, Rusakova IA, et al. Bismuth@US-tubes as a potential contrast agent for X-ray imaging applications. Journal of Materials Chemistry B 2013;1:4792-800.

[9]Hong SY, Tobias G, Al-Jamal KT, Ballesteros B, Ali-Boucetta H, Lozano-Perez S, et al. Filled and glycosylated carbon nanotubes for in vivo radioemitter localization and imaging. Nat Mater 2010;9:485-90.

[10]   Serpell CJ, Rutte RN, Geraki K, Pach E, Martincic M, Kierkowicz M, et al. Carbon nanotubes allow capture of krypton, barium and lead for multichannel biological X-ray fluorescence imaging. 2016;7:13118.

[11]   Shearer CJ, Cherevan A, Eder D. Application and Future Challenges of Functional Nanocarbon Hybrids. Advanced Materials 2014;26:2295-318.

[12]   del Carmen Giménez-López M, Moro F, La Torre A, Gómez-García CJ, Brown PD, van Slageren J, et al. Encapsulation of single-molecule magnets in carbon nanotubes. Nat Commun 2011;2:407.

[13]   Martincic M, Tobias G. Filled carbon nanotubes in biomedical imaging and drug delivery. Expert Opinion on Drug Delivery 2015;12:563-81.

[14]   Wang T, Fu Y, Chai L, Chao L, Bu L, Meng Y, et al. Filling Carbon Nanotubes with Prussian Blue Nanoparticles of High Peroxidase-Like Catalytic Activity for Colorimetric Chemo- and Biosensing. Chemistry – A European Journal 2014;20:2623-30.

[15]   Chuvilin A, Bichoutskaia E, Gimenez-Lopez MC, Chamberlain TW, Rance GA, Kuganathan N, et al. Self-assembly of a sulphur-terminated graphene nanoribbon within a single-walled carbon nanotube. Nat Mater 2011;10:687-92.

[16]   Wang Z, Li H, Liu Z, Shi Z, Lu J, Suenaga K, et al. Mixed low-dimensional nanomaterial: 2D ultranarrow MoS_2 inorganic nanoribbons encapsulated in quasi-1D carbon nanotubes. Journal of the American Chemical Society 2010;132:13840-7.

[17]   Cabana L, Ballesteros B, Batista E, Magén C, Arenal R, Oró-Solé J, et al. Synthesis of PbI_2 Single-Layered Inorganic Nanotubes Encapsulated Within Carbon Nanotubes. Advanced Materials 2014;26:2016–21.

[18]   Zhou M, Duan W, Chen Y, Du A. Single layer lead iodide: computational exploration of structural, electronic and optical properties, strain induced band modulation and the role of spin-orbital-coupling. Nanoscale 2015;7:15168-74.

[19]   Rao CNR, Govindaraj A. Synthesis of Inorganic Nanotubes. Advanced Materials 2009;21:4208-33.

[20]   Goldberger J, Fan R, Yang P. Inorganic Nanotubes: A Novel Platform for Nanofluidics. Accounts of Chemical Research 2006;39:239-48.

[21]   Al-Dulaimi N, Lewis EA, Lewis DJ, Howell SK, Haigh SJ, O'Brien P. Sequential bottom-up and top-down processing for the synthesis of transition metal dichalcogenide nanosheets: the case of rhenium disulfide (ReS2). Chemical Communications 2016;52:7878-81.

[22] Feng W, Zhenxing W, Qisheng W, Fengmei W, Lei Y, Kai X, et al. Synthesis, properties and applications of 2D non-graphene materials. Nanotechnology 2015;26:292001.

[23] Naguib M, Mochalin VN, Barsoum MW, Gogotsi Y. 25th Anniversary Article: MXenes: A New Family of Two-Dimensional Materials. Advanced Materials 2014;26:992-1005.

[24] Hwang DY, Choi KH, Park JE, Suh DH. Highly thermal-stable paramagnetism by rolling up MoS2 nanosheets. Nanoscale 2017;9:503-8.

[25] Mohammad HT, Volker JS. Enhanced photon absorption in spiral nanostructured solar cells using layered 2D materials. Nanotechnology 2015;26:344005.

[26] Liu P, Jin Z, Katsukis G, Drahushuk LW, Shimizu S, Shih C-J, et al. Layered and scrolled nanocomposites with aligned semi-infinite graphene inclusions at the platelet limit. Science 2016;353:364.

[27] Soto Lamata I, Alonso-González P, Hillenbrand R, Nikitin AY. Plasmons in Cylindrical 2D Materials as a Platform for Nanophotonic Circuits. ACS Photonics 2015;2:280-6.

[28] Cabana L, Ke X, Kepić D, Oro-Solé J, Tobías-Rossell E, Van Tendeloo G, et al. The role of steam treatment on the structure, purity and length distribution of multi-walled carbon nanotubes. Carbon 2015;93:1059-67.

[29] Ballesteros B, Tobias G, Shao L, Pellicer E, Nogués J, Mendoza E, et al. Steam Purification for the Removal of Graphitic Shells Coating Catalytic Particles and the Shortening of Single-Walled Carbon Nanotubes. Small 2008;4:1501-6.

[30] Sloan J, Kirkland AI, Hutchison JL, Green MLH. Integral atomic layer architectures of 1D crystals inserted into single walled carbon nanotubes. Chemical Communications 2002:1319-32.

[31] Handbook of Chemistry and Physics. 84th ed: CRC Press 2003-2004.

[32] Asprey LB, Keenan TK, Kruse FH. Preparation and Crystal Data for Lanthanide and Actinide Triiodides. Inorganic Chemistry 1964;3:1137-41.

[33] Brown G, Bailey SR, Novotny M, Carter R, Flahaut E, Coleman KS, et al. High yield incorporation and washing properties of halides incorporated into single walled carbon nanotubes. Appl Phys A 2003;76:457-62.

[34] Aqra F. Surface tension of molten metal halide salts. Journal of Molecular Liquids 2014;200, Part B:120-1.

[35] de Jongh PE, Eggenhuisen TM. Melt Infiltration: an Emerging Technique for the Preparation of Novel Functional Nanostructured Materials. Advanced Materials 2013;25:6672-90.

[36] Nellist PD, Pennycook SJ. Direct Imaging of the Atomic Configuration of Ultradispersed Catalysts. Science 1996;274:413-5.

[37] Luksirikul P, Ballesteros B, Tobias G, Moloney MG, Green MLH. Sidewall functionalisation of carbon nanotubes by addition of diarylcarbene derivatives. Journal of Materials Chemistry 2011;21:19080-5.

[38] Hulliger F. Structural chemistry of layer-type phases. Holland: D. Reidel Publishing Company 1976.

[39] Yamaguchi S. Determining the crystal structure of hygroscopic substances by Electron Diffraction (continued): Zn I2. Scientific Papers of the Institute of Physical and Chemical Research 1942;39:357-9.

[40] Gunsilius H, Borrmann H, Simon A, Urland W. Zur Polymorphie von TbCl3. Allemand 1988;43:1023-8.

[41] Kreizman R, Hong SY, Sloan J, Popovitz-Biro R, Albu-Yaron A, Tobias G, et al. Core–Shell PbI2@WS2 Inorganic Nanotubes from Capillary Wetting. Angewandte Chemie International Edition 2009;48:1230-3.

- Supporting Information -

Encapsulation of two-dimensional materials inside carbon nanotubes: towards an enhanced synthesis of single-layered metal halides

Stefania Sandoval, Elzbieta Pach, Belén Ballesteros and Gerard Tobias
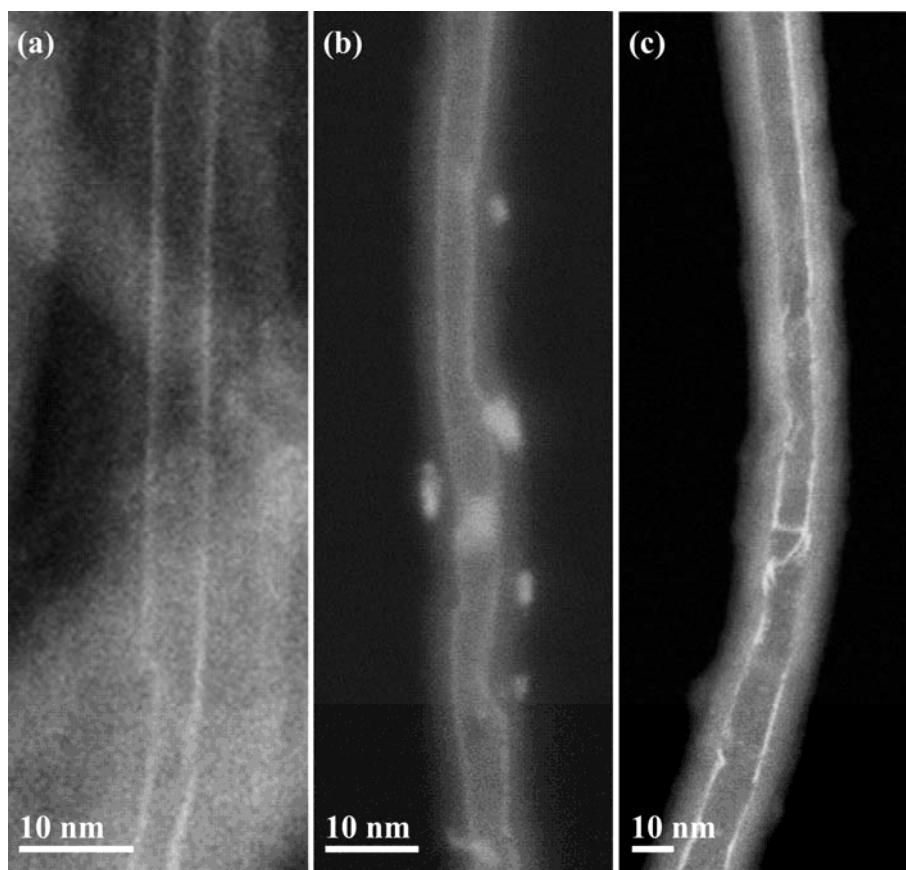
Additional analyses of the prepared materials

Figure S1. HAADF-STEM images of (a) CeI_3 (b)$TbCl_3$ and (c) ZnI_2 nanotubes confined within MWCNTs. The ZnI_2 nanotube presents a closing in the middle of the structure.
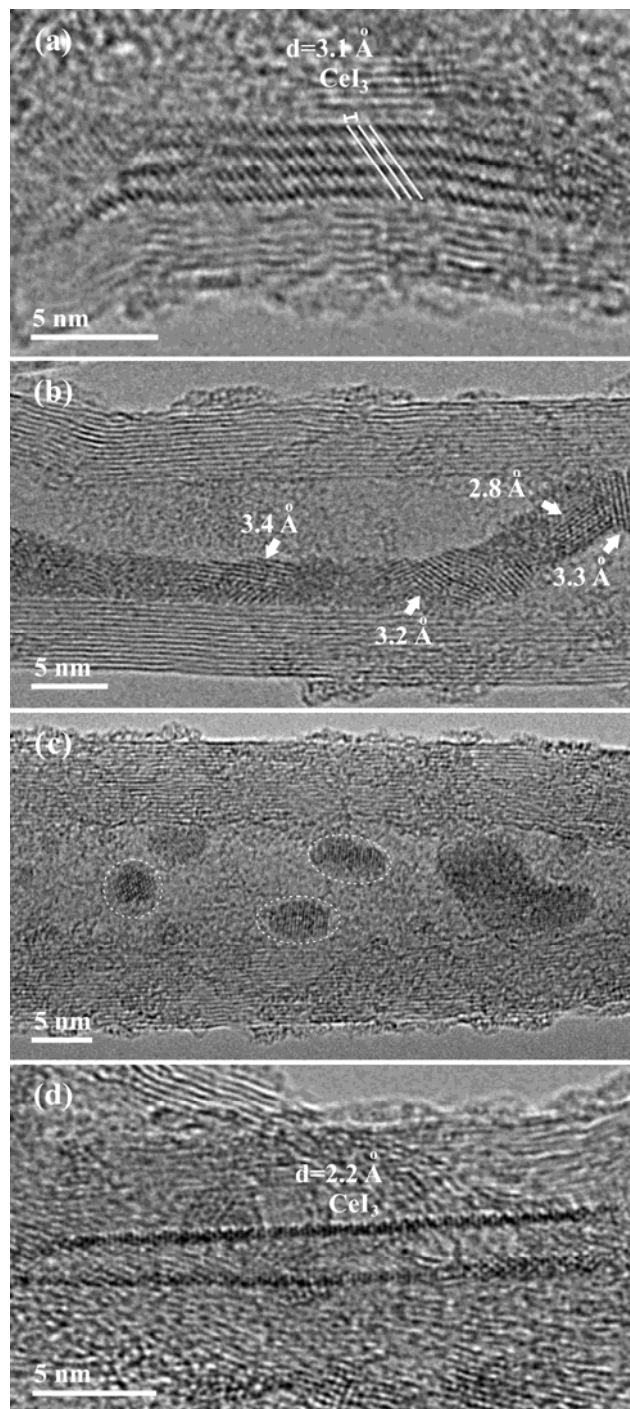
Figure S2. High resolution transmission electron microscopy (HRTEM) images of MWCNTs filled with (a) a CeI₃ nanorod, (b) a CeI₃ "nanosnake", (c) ZnI₂ nanoparticles and (d) a CeI₃ nanotube.
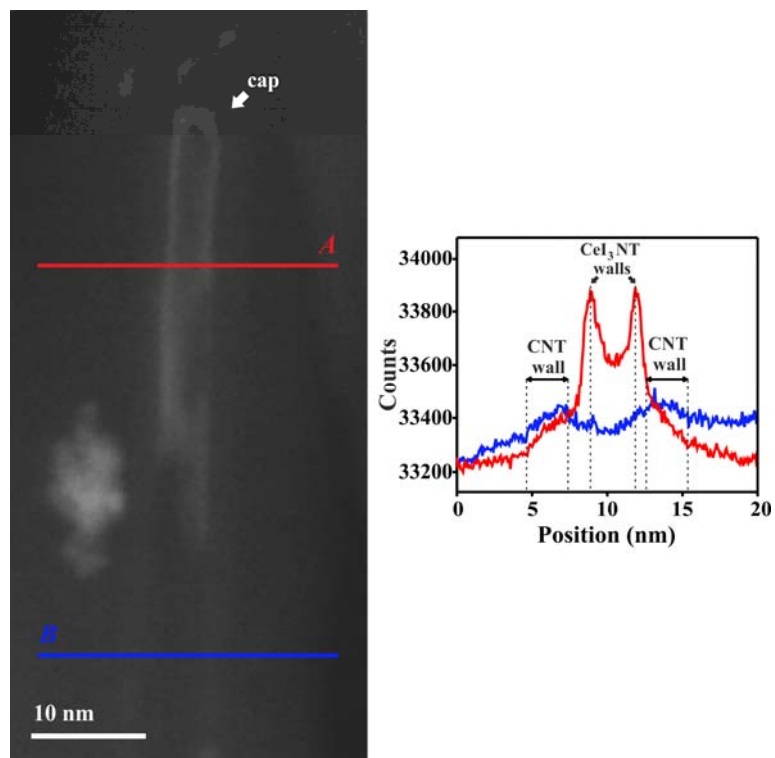
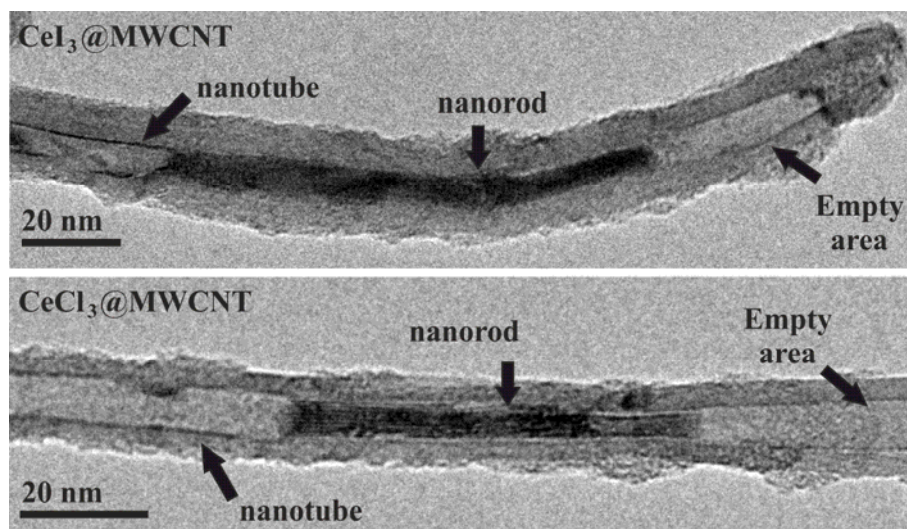**Figure S3.** Intensity profile of a CeI_3 closed tube.

Figure S4. TEM image showing the simultaneous presence of a CeI_3 nanotube and a nanorod inside the same MWCNT. The higher contrast on the edges when a nanotube is present allows the differentiation between the grown tubular structure and the empty area.
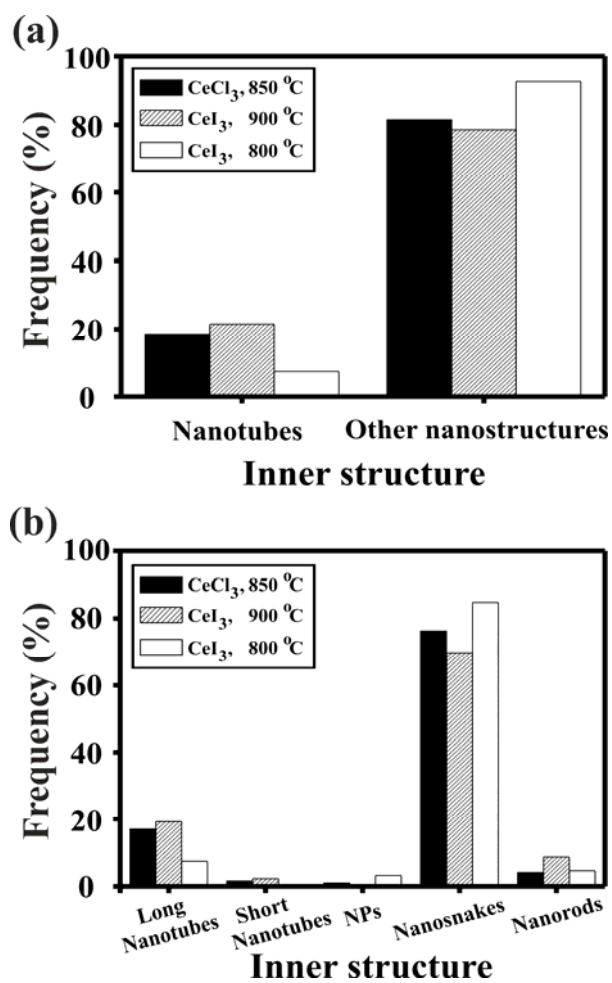
Figure S5. Bar diagram showing the distribution (frequency, %) of the different $CeCl_3$ and CeI_3 nanostructures grown inside MWCNTs. For numerical data see Tables S1 and S2.
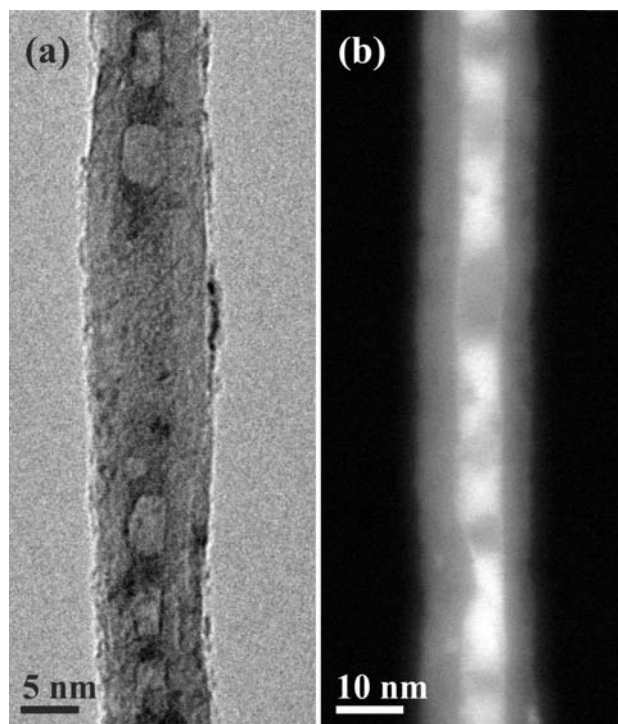
Figure S6. Short single-layered nanotubes grown within MWCNTs **(a)** TEM image of $CeCl_3$ and **(b)** HAADF STEM image of $TbCl_3$.

Table S1. Nanostructres formed by molten phase filling of MWCNTs with CeI_3, $CeCl_3$ and ZnI_2 at different temperatures.

| Sample	# of filled MWCNTs	Long Nanotubes	Short Nanotubes	Nanoparticles (NPs)	"Nanosnakes"	Nanorods
CeI_3, 800 ºC	217	16	--	7	184	10
	100%	**7.4%**	**--**	**3.2%**	**84.8%**	**4.6%**
CeI_3, 900 ºC	219	42	5	--	153	19
	100%	**19.2%**	**2.3%**	**--**	**69.8%**	**8.7%**
$CeCl_3$, 850 ºC	578	98	9	6	441	24
	100%	**17%**	**1.6%**	**1%**	**76.3%**	**4.1%**
ZnI_2, 475 ºC	443	70	25	--	324	24
	100%	**15.8%**	**5.6%**	**--**	**73.2%**	**5.4%**
ZnI_2, 575 ºC	426	72	38	--	258	58
	100%	**16.9%**	**8.9%**	**--**	**60.6**	**13.6%**
ZnI_2, 700 ºC	328	86	38	--	94	110
	100%	**26.2%**	**11.6%**	**--**	**28.7**	**33.5%**
ZnI_2, 1000 ºC	191	116	8	1	39	27
	100%	**60.7**	**4.2%**	**0.5**	**20.4**	**14.2%**
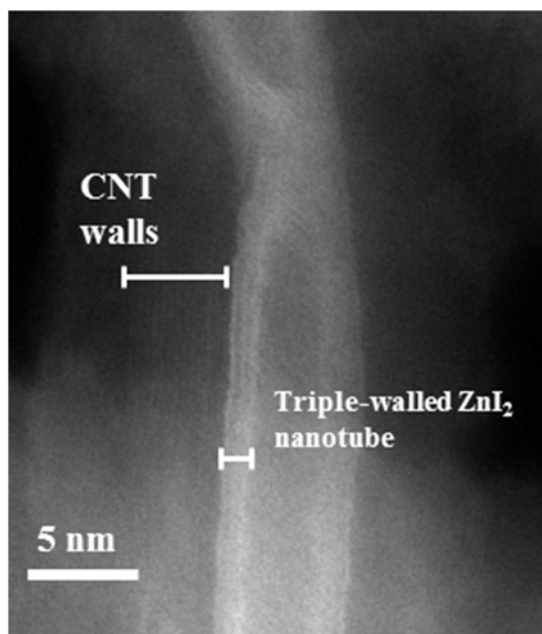
Figure S7. HAADF STEM image of a triple-walled ZnI_2 nanotube inside the cavities of a MWCNTs.
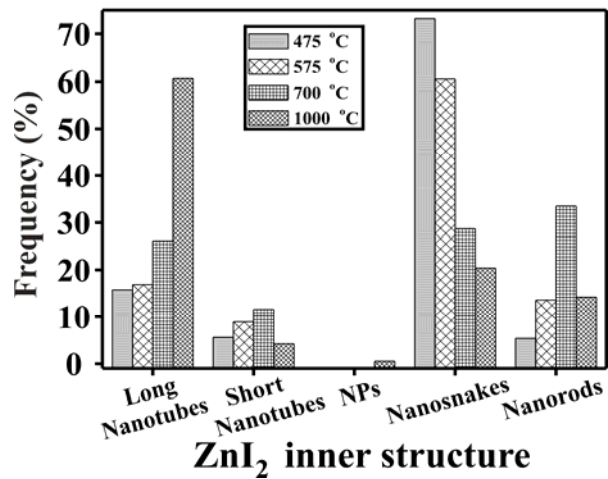

Figure S8. Bar diagram showing the distribution (frequency, %) of the different ZnI_2 nanostructures grown inside MWCNTs.